Influence of ferromagnetic layer thickness on the magnetic properties of Cr/$Fe_{1-x}Co_x$ bilayers

S. MICAN[a,*], D. BENEA[a], A. TAKÁCS[a], E. MOSSANG[b,c], O. ISNARD[b,c], V. POP[a]
[a]*Babeş-Bolyai University, Faculty of Physics, 1 M. Kogălniceanu, 400084, Cluj-Napoca, Romania*
[b]*Université Grenoble Alpes, Institut Néel, 25 Rue des Martyrs, F-38042, Grenoble, France*
[c]*CNRS, Institut Néel, 25 Rue des Martyrs, F-38042, Grenoble, France*

The influence of $Fe_{1-x}Co_x$ thickness on the magnetic properties of Cr/$Fe_{1-x}Co_x$ bilayers is investigated. Electronic structure calculations showed that the Cr moments are suppressed by Co addition and by the deposition of multiple $Fe_{1-x}Co_x$ layers. Cr/$Fe_{65}Co_{35}$ bilayers were studied experimentally. Structural investigations showed the presence of strain and a rough Cr/$Fe_{65}Co_{35}$ interface in the measured samples. The magnetic data was analyzed using the Mauri-Siegmann model, which showed that the interfacial Cr moments decrease with increasing $Fe_{65}Co_{35}$ thickness. A large bias field of 0.09T was found at 4K for the sample with a 10 nm thick $Fe_{65}Co_{35}$ layer, around 10 times larger than previous reports.

(Received June 25, 2018; accepted June 14, 2019)

Keywords: Thin films, Cr/Fe-Co bilayers, Band structure calculations, Magnetic measurements, Exchange bias

1. Introduction

Multilayer systems comprised of magnetic and non-magnetic layers have been intensely studied due to their scientific and technological relevance. Magnetic multilayers exhibit special or enhanced physical properties, such as giant magnetoresistance, a discovery which led to the development of spin valves, magnetoresistive random-access memory (MRAM), magnetic tunnel junctions and spintronics [1-6].

Systems composed of a ferromagnetic (FM) layer deposited on a Cr underlayer exhibit many interesting properties. Unlike common antiferromagnets like CoO and MnO which show an antiparallel ordering of localized moments, Cr is an itinerant spin density wave (SDW) antiferromagnet (AFM) [7]. Bulk Cr orders in an incommensurate spin-density wave (ISDW), where the magnitude of the sublattice spins, $\mathbf{S}_{AFM}$ is modulated sinusoidally [8, 9]. The ISDW was described through a wave vector $\mathbf{Q}$, which has a wavelength $\lambda = 2\pi/|\mathbf{Q}|$. The wavelength is incommensurate with the periodicity of the crystal lattice [8]. Two ISDW phases are present below the Neel temperature, T_N: a high temperature transverse phase, where $\mathbf{Q} \perp \mathbf{S}_{AFM}$, and a low temperature longitudinal phase, where $\mathbf{Q} \parallel \mathbf{S}_{AFM}$ [8, 9]. The two phases are separated by a spin-flip transition temperature, T_{SF}, of 123 K [9]. The finite-size confinement in thin films leads to interesting behaviors very different from the bulk, such as oscillatory coupling [10], spin-dependent interfacial scattering [11], surface spin flops [12], and biquadratic coupling [13]. The onset thickness of finite-size effects in Cr was reported to be around 110 nm [8].

It was suggested that the exchange bias could be used to probe the magnetic behavior of the interface in Cr/FM systems [8]. First discovered by Meiklejohn and Bean [14], exchange bias is determined by the interfacial coupling between an FM and AFM layer, and it manifests itself as the shift of a magnetic hysteresis loop along the field axis, and, in special cases, along the moment axis [5, 15]. The size of the bias depends on several factors, such as the magnetic spin moments of both the AFM and FM interface layers, the AFM/FM exchange coupling, FM magnetization, AFM/FM layer thickness, the ISDW in the antiferromagnet, frustration effects at the interface, anisotropy and cooling field [1, 4, 5, 7, 15-18].

The magnetic properties of Cr/FM multilayers were studied in both epitaxial and polycrystalline systems, where the ferromagnetic material was either Fe, Co, or permalloy [4, 7, 8, 11-13, 19, 20]. However, most of the studies were mainly focused on the evolution of the magnetic properties of the film with Cr thickness. For example, an increase in both bias and coercive field values with Cr thickness was reported in polycrystalline permalloy films covered with Cr, however, the field values decreased with temperature [7]. On the other hand, it was reported that in epitaxial Fe/Cr films, the bias field has an oscillatory dependence on the temperature [8]. In addition to the AFM layer thickness, the FM layer thickness can also affect the magnetic properties of the Cr underlayer through interfacial exchange [15]. Furthermore, a large FM magnetization could enhance the bias field [15]. For instance, in polycrystalline ferromagnetic films (permalloy or Co) covered with Cr, an inversely proportional dependence of the bias field on the ferromagnetic layer thickness was reported [7]. Also, the permalloy/Cr films showed larger bias field values than the Co/Cr ones [7]. Among the multitude of existing ferromagnets, one material of interest is the $Fe_{65}Co_{35}$ alloy (called "permendur"), which has the largest 3*d* magnetic moment in the Fe-Co series and the highest known room-

temperature magnetization value of 2.43 T [21-24]. In this work we investigate the influence of $Fe_{65}Co_{35}$ thickness on the magnetic properties of Cr(100 nm)/$Fe_{65}Co_{35}$(10-100 nm) bilayers. First, we investigated, through electronic structure calculations, the effect of Co addition on the magnetic properties of a Cr/Fe bilayer system, as well as the effect of depositing multiple atomic layers of $Fe_{1-x}Co_x$ on a Cr underlayer. The evolution of the interface magnetic moments is of particular interest. Secondly, the evolution of the magnetic properties and exchange bias of the sputtered Cr/$Fe_{65}Co_{35}$ bilayers was investigated as a function of $Fe_{65}Co_{35}$ thickness and temperature by means of magnetic hysteresis measurements. The exchange bias was analyzed using a simple model developed by Mauri et al. [18], in conjunction with experimental data and theoretical results. We will show that the inversely proportional dependence of the bias field on the $Fe_{65}Co_{35}$ layer thickness is determined by the progressive damping of the interface Cr moments as more ferromagnetic layers are deposited.

2. Materials and methods

2.1. Computational details

The correlation between the structure and magnetism for 3*d* metals has been investigated using the tight-binding-KKR (Korringa-Kohn-Rostoker) band structure calculation method [25]. The SPR-TB-KKR program package allows dealing with 3D- and 2D-systems making use of the screened or tight binding KKR formalism [26]. The calculations were done in spin-polarized fully-relativistic mode, using CPA alloy theory, in ferromagnetic and antiferromagnetic spin configurations. The local spin density approximation (LSDA) for the exchange-correlation energy was used with the parametrization of Vosko, Wilk and Nusair (VWN) [27].

Electronic structure calculations have been performed for configurations consisting of 1, 2, and 4 monolayers (ML) of $Fe_{1-x}Co_x$ (x = 0, 0.34, and 0.50) grown on top of bulk Cr oriented in the (100) direction. The magnetic moments are given for the interface region, which is comprised of the deposited $Fe_{1-x}Co_x$ layers along with 4 ML of Cr. The experimental lattice parameter of Cr was used in the calculations.

2.2. Experimental details

Bilayer configurations consisting of Cr(100 nm)/$Fe_{65}Co_{35}$(10-100 nm) were deposited using DC magnetron sputtering onto Si(100) substrates coated with 100 nm of SiO_2. Prior to deposition, the substrates were cleaned in an ultrasonic bath for 5 minutes in acetone, followed by ethanol, and distilled water. The base pressure was $7 \cdot 10^{-7}$ mbar. The Ar pressure during deposition was kept at 3.4 mTorr for Cr and 1.5 mTorr for $Fe_{65}Co_{35}$, while the sputtering power was kept at 30 W. The film thickness was monitored during deposition using an Inficon SQM-160 rate/thickness monitor previously calibrated by X-ray reflectivity.

The layer thickness and interface roughness were measured using the X-ray reflectivity (XRR) technique, while the crystal structure was investigated using grazing incidence X-ray diffraction (XRD). The XRR and grazing incidence XRD measurements were performed using a Bruker D8 Discover diffractometer with Cu K_α radiation. The X-ray reflectivity curves were fitted using the GenX software [28], a versatile program which uses the differential evolution algorithm to fit XRR data. The phase analysis and lattice parameter determination were done using the Powdercell software.

Magnetic measurements were performed using a vibrating sample magnetometer (VSM) in the temperature range 4-300 K and applied fields up to 1 T. The magnetic field was always applied parallel to the sample surface.

3. Results and discussions

3.1. Electronic structure calculations

Band structure calculations have been performed in order to clarify the evolution of the magnetic properties of the Cr/$Fe_{1-x}Co_x$ films as a function of ferromagnetic layer thickness. Firstly, we will examine the magnetic evolution of $Fe_{1-x}Co_x$ as more layers are deposited. Secondly, we will investigate the effect which the deposited ferromagnetic layers have on the magnetism of the Cr underlayer.

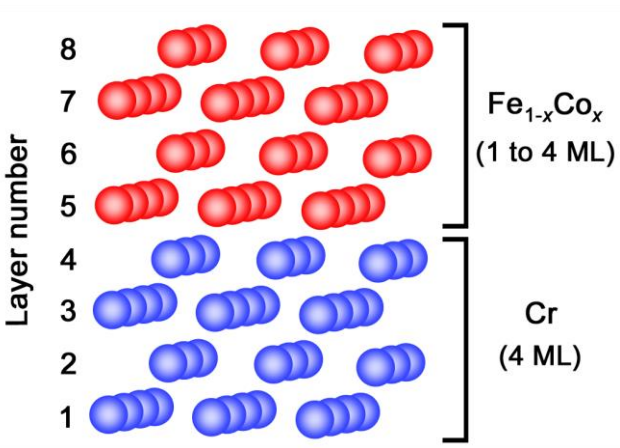

Fig. 1. Representation of the $Fe_{1-x}Co_x$/Cr(100) layer configurations used in the calculations

Configurations were constructed, consisting of 1, 2, and 4 ML of $Fe_{1-x}Co_x$ (x = 0, 0.34, and 0.50) grown on bulk Cr oriented in the (100) direction – Fig. 1. Layers 1 to 4 form the Cr interface layers, while layers 5 to 8 contain $Fe_{1-x}Co_x$. The layer-resolved magnetic moments for the systems consisting of 1 ML, 2 ML, and 4 ML of $Fe_{1-x}Co_x$ on Cr (x = 0, 0.34, and 0.50) are given in Table 1.

For the configuration consisting of 1 ML of Fe deposited on Cr, the Fe magnetic moment, 2.29 μ_B/atom is higher than the bulk value. A spin moment of 2.19 μ_B and an increased orbital moment of 0.10 μ_B were found,

suggesting a higher anisotropy than the bulk. The larger magnetic moment of Fe can be attributed to the finite size of the Fe layer as there are no neighbouring atoms above it. Consequently, this removes the orbital quenching usually observed in high symmetry bulk 3*d* transition metals. For example, a Fe moment of 2.28 μ_B/atom was reported for ultrafine particles 1.8 nm in size [29].

By adding Co we obtain the systems consisting of 1 ML of $Fe_{1-x}Co_x$ on Cr. In this case, the Fe magnetic moment increases with Co content, but the values are smaller than those reported for bulk $Fe_{1-x}Co_x$ [21]. The Co magnetic moments are much smaller than the ones obtained in bulk $Fe_{1-x}Co_x$ [21]. It is interesting to note that for x = 0.34, we have a ferromagnetic coupling between Fe and Co, while for x = 0.50 Fe and Co are unexpectedly antiferromagnetically coupled. We can analyze this behavior by looking at the magnetic moments of Fe, Co and Cr in the interface layers.

Table 1. The layer-resolved magnetic moments of Cr, Fe and Co for the configurations consisting of 1 ML of Fe on Cr(100) and 1, 2, and 4 ML of $Fe_{1-x}Co_x$ on Cr(100)

Layer number	**Atom**	***M* (μ_B/atom)**						
		***x* = 0**	***x* = 0.34**			***x* = 0.50**		
		1 ML	**1 ML**	**2 ML**	**4 ML**	**1 ML**	**2 ML**	**4 ML**
8	Fe	-	-	-	3.00	-	-	2.98
	Co	-	-	-	1.89	-	-	1.89
7	Fe	-	-	-	2.49	-	-	2.53
	Co	-	-	-	1.73	-	-	1.74
6	Fe	-	-	3.00	2.65	-	3.01	2.68
	Co	-	-	1.90	1.73	-	1.89	1.73
5	Fe	2.29	2.37	1.85	2.03	2.50	1.92	2.05
	Co	-	0.25	1.38	1.10	-0.73	1.16	1.09
4	Cr	-1.15	-0.68	-0.64	-0.20	-0.85	-0.27	-0.25
3	Cr	1.05	0.51	0.41	0.17	0.87	0.14	0.20
2	Cr	-0.79	-0.36	-0.40	-0.12	-0.65	-0.14	-0.16
1	Cr	0.53	0.22	0.20	0.08	0.47	0.08	0.08

For x = 0.34 Co has a very small moment of 0.25 μ_B/atom. By increasing the Co concentration to x = 0.50, the Co moment reverses and increases to -0.75 μ_B/atom. With increasing Co content, for 1 ML of $Fe_{1-x}Co_x$ on Cr, the Cr interface moment initially drops (x = 0.34), then increases again (x = 0.50). Also, the addition of Co diminishes the Cr interface moments compared to the case of pure Fe on Cr. It appears that Cr increasingly polarizes the Co moment as the Fe concentration in the interface layer decreases. On the other hand, the magnetic moments of Fe in the system of 1 ML of $Fe_{1-x}Co_x$ on Cr have a behavior similar to the one found in bulk $Fe_{1-x}Co_x$ [21].

In the system consisting of 2 ML of $Fe_{1-x}Co_x$ on Cr, the Fe moment in the interface layer decreases, while the Co interface moment increases compared to the previous case of 1 ML of $Fe_{1-x}Co_x$ on Cr. Interestingly, in the topmost layer, the Fe and Co moments have rather large values, much larger than the bulk [21]. Increasing the Co concentration leads to a small increase of the Fe moments and a very small decrease of the Co moments, in agreement with previous results [21].

For 4 ML of $Fe_{1-x}Co_x$ on Cr, the magnetic moments of Fe and Co on the topmost layer stay close to the previous values obtained for 2 ML of $Fe_{1-x}Co_x$ on Cr, while in the interface layer, the Fe and Co moments suffer only small variations. In the layers between the interface and the topmost layer, Fe and Co have magnetic moments close to the bulk [21]. From this we can deduce that the magnetic moments in the topmost layer are mostly affected by reduced coordination, while the interface layer is influenced by both the Cr atoms from the underlayer and Fe/Co atoms deposited on top. This reflects the large sensitivity of the magnetic moment magnitude to the local atomic environment in the thin layers, a sensitivity also reported for metallic Fe in bulk intermetallic compounds [30].

The total magnetic moment of each layer, in μ_B/f.u., as a function of layer number for the systems consisting of 1 ML of $Fe_{1-x}Co_x$ on Cr (x = 0, 0.34 and 0.50) and 4 ML of $Fe_{1-x}Co_x$ on Cr (x = 0.34 and 0.50) are shown in Figures 2a and 2b respectively. The Cr underlayer shows a spin-density wave (SDW) behaviour, the Cr magnetic moments decreasing in amplitude as the distance from the interface increases.

The addition of Co reduced the Cr moments – Fig. 2a – the maximum damping being obtained for x = 0.34.

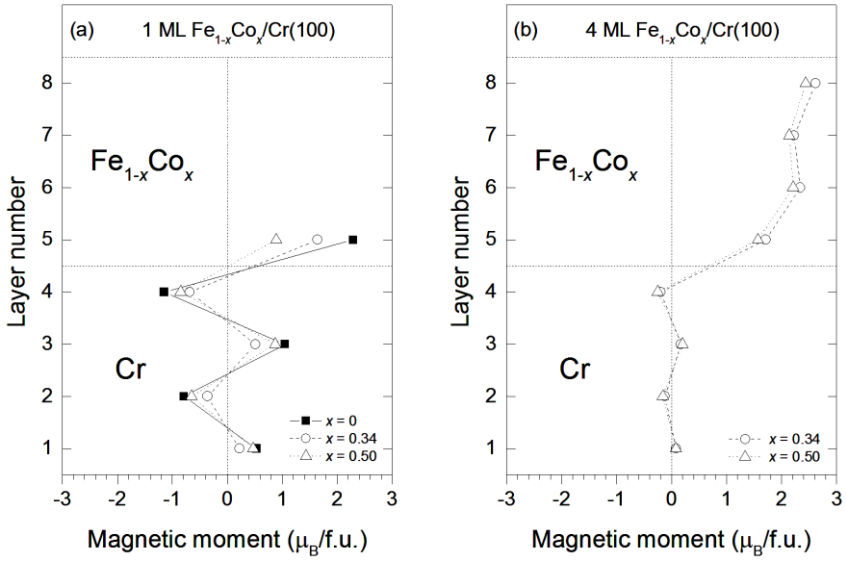

Fig. 2. Layer-resolved Cr and $Fe_{1-x}Co_x$ magnetic moments as a function of Co content for (a) 1 ML of $Fe_{1-x}Co_x$ on Cr and (b) 4 ML of $Fe_{1-x}Co_x$ on Cr

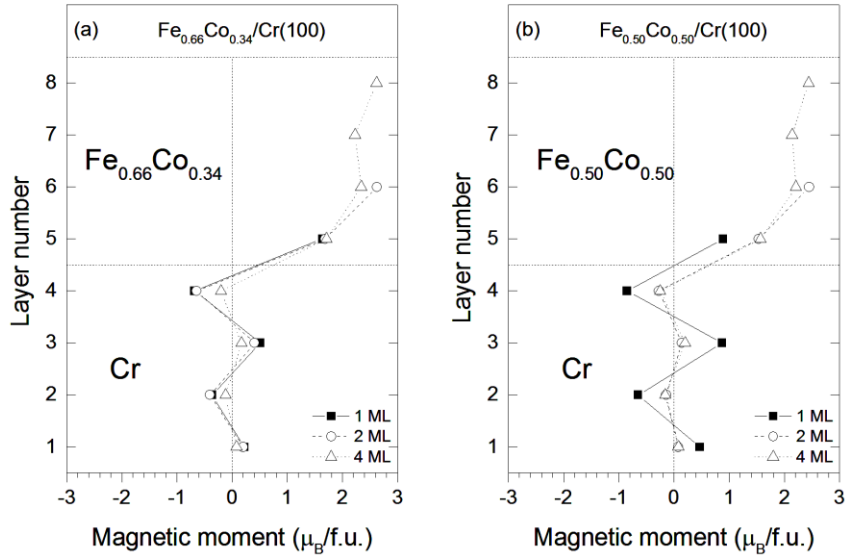

Fig. 3. Layer-resolved Cr and $Fe_{1-x}Co_x$ magnetic moments for 1, 2 and 4 ML of $Fe_{0.66}Co_{0.34}$ on Cr (a) and $Fe_{0.50}Co_{0.50}$ on Cr (b)

One could observe that the ferromagnetic layer moments are smaller for $x = 0.50$ compared to $x = 0.34$ – Fig. 2b – in agreement with the Slater-Pauling curve obtained for $Fe_{1-x}Co_x$ [21].

The Cr underlayers are also affected by the number of deposited Fe-Co layers, as shown in Figures 3a and 3b. It can be seen that the Cr magnetic moments are progressively reduced when the number of deposited $Fe_{1-x}Co_x$ layers increases. As we have discussed earlier, the Cr-Co exchange interaction competes with the Fe-Co interaction. For 1 ML of $Fe_{1-x}Co_x$ on Cr, the Cr underlayer had a predominant effect on the Co moments. As more layers are added, the Fe-Co interaction becomes dominant, leading to a damping of the Cr magnetic moments through the Cr-Co exchange interaction.

3.2. XRR and XRD investigations

In order to investigate the thickness of the deposited bilayer configurations, we employed the X-ray reflectivity technique, which can give us information regarding film thickness and interface roughness. The measured XRR curves were then fitted using the GenX software [28]. For the XRR fits we used a multilayer model in which we assumed homogeneous layers with interface roughness and interdiffusion. For the starting model used in the fits, the substrate was considered to be pure Si. The 1st layer was comprised of 100 nm of SiO_2, the 2nd layer consisted of 100 nm of Cr, while the 3rd layer contained 10 to 100 nm of $Fe_{65}Co_{35}$. A thin 1 nm layer of Fe_2O_3 was added on top of the starting multilayer model, as the measurements and sample handling were performed in air.

The measured X-ray reflectivity curves for the deposited samples along with the fitted curves are shown in Fig. 4. It can be seen that the simulated XRR curves fit the measured curves reasonably well, meaning the model used is close to the real configuration of the samples. The results of the fits are shown in Table 2. The thickness values obtained from the fits are close to the desired thickness configurations. A very thin surface layer of Fe_2O_3 was found in the investigated samples, mainly due to their manipulation in air. A root mean square roughness value around 3 nm was obtained for the Cr/$Fe_{65}Co_{35}$ interface for all of the samples. This is also confirmed by the absence of oscillations in reflectivity – Fig. 4 – which is an indicative of a rough interface. This behavior is unavoidable in polycrystalline sputtered films [31].

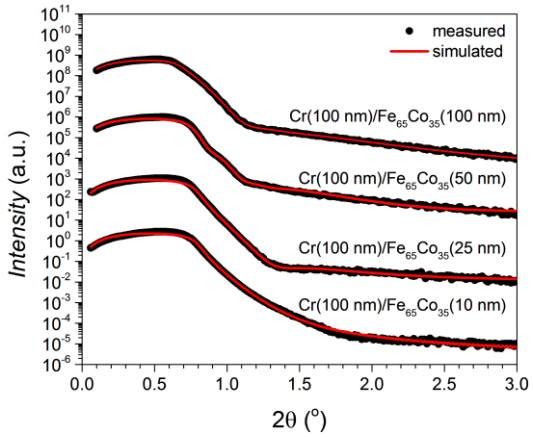

Fig. 4. Measured and simulated X-ray reflectivity curves for the deposited bilayer samples. The symbols represent measured data, while the red lines represent the fitted reflectivity curves. The measurements were performed using Cu K_α radiation

Table 2. Thickness values obtained from the XRR fits for the SiO_2 underlayer, t_{SiO2}, the Cr layer, t_{Cr}, the $Fe_{65}Co_{35}$ layer, $t_{Fe65Co35}$, and the Fe_2O_3 layer, t_{Fe2O3}. The root mean square roughness values of the Cr/$Fe_{65}Co_{35}$ interface, $\sigma_{Cr/Fe65Co35}$, are also given

Desired configuration	t_{SiO2} (nm)	t_{Cr} (nm)	$t_{Fe65Co35}$ (nm)	t_{Fe2O3} (nm)	$\sigma_{Cr/Fe65Co35}$ (nm)
Cr (100 nm)/$Fe_{65}Co_{35}$ (100 nm)	95 ± 2	103 ± 2	102 ± 5	2 ± 0.2	3.1 ± 0.6
Cr (100 nm)/$Fe_{65}Co_{35}$ (50 nm)	104 ± 3	108 ± 10	58 ± 3	0 ± 0.2	3.2 ± 2
Cr (100 nm)/$Fe_{65}Co_{35}$ (25 nm)	104 ± 2	99 ± 3	20 ± 1	3.4 ± 0.1	2.9 ± 0.5
Cr (100 nm)/$Fe_{65}Co_{35}$ (10 nm)	104 ± 2	105 ± 10	9 ± 0.3	0.6 ± 0.03	2.5 ± 0.2

The grazing incidence X-ray diffraction patterns are shown in Fig. 5. The grazing incidence scans were performed as 2θ detector scans at fixed source θ values of 1.5 – Fig. 5 (a) – and 0.8 degrees – Fig. 5 (b). For θ = 1.5 degrees the Cr/$Fe_{65}Co_{35}$ (110) peak is visible along with the (311) peak coming from the Si substrate and the (221) and (301) peaks of α-cristobalite [32] originating from the SiO_2 underlayer. By scanning at a lower θ angle of 0.8 degrees, the only observable peaks are the (110) peak of Cr/$Fe_{65}Co_{35}$ and a faint (311) peak from the Si substrate. These observations lead us to believe that our bilayer samples are textured along the (110) direction. Texturing along a specific direction is common for polycrystalline films deposited at room temperature and low sputtering power [33-35]. Since Cr and $Fe_{65}Co_{35}$ have the same BCC crystal structure with a very good lattice parameter matching, the (110) peak of $Fe_{65}Co_{35}$ is superimposed on the (110) peak of Cr. Even though it is difficult to separate the two contributions to the (110) reflection, by taking into account the low mismatch between Cr and $Fe_{65}Co_{35}$, we can infer that $Fe_{65}Co_{35}$ grows in tune with the Cr layer and they are both textured along the (110) direction.

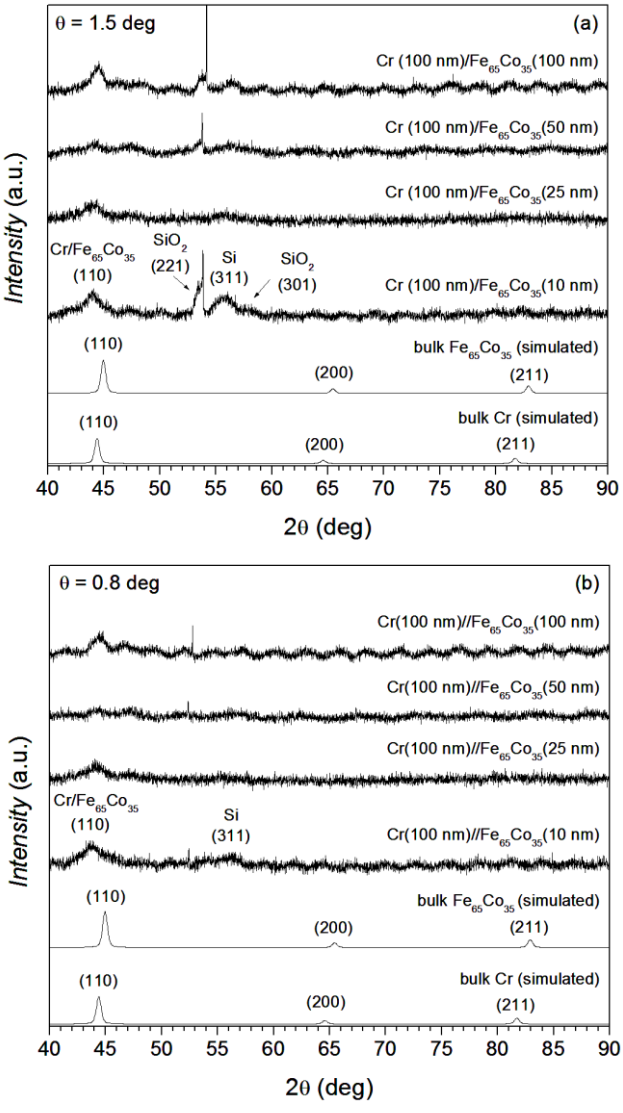

Fig. 5. Grazing incidence XRD patterns measured at $\theta = 1.5^o$ (a) and $\theta = 0.8^o$ (b). The simulated patterns of bulk Cr and $Fe_{65}Co_{35}$ are shown for comparison. The measurements were performed using Cu K_α radiation

By looking at the diffraction patterns in Figures 5 (a) and (b) we can see that the (110) reflections of Cr/$Fe_{65}Co_{35}$ progressively shift to higher 2θ angles as the $Fe_{65}Co_{35}$

thickness increases. As Cr and $Fe_{65}Co_{35}$ have BCC unit cells, the 2θ shift translates into a decrease of the lattice parameter of the film. Table 3 shows the lattice parameters of the investigated samples obtained from grazing incidence XRD scans. We can see that for the thinnest film configuration, 10 nm of $Fe_{65}Co_{35}$ on 100 nm of Cr, the lattice parameter, 2.92 Å, is larger than that of bulk Cr, 2.88 Å [36]. This is an indication of strain in our samples, possibly induced by the crystalline SiO_2 underlayer. As the thickness of the $Fe_{65}Co_{35}$ layer increases, the lattice parameter decreases. The lowest value of 2.88 Å was obtained for the configuration consisting of 100 nm of $Fe_{65}Co_{35}$ on 100 nm of Cr. However, this value is still larger than the one obtained for bulk $Fe_{65}Co_{35}$, of 2.85 Å. Therefore, even as strain is relaxed with increasing $Fe_{65}Co_{35}$ thickness, it is not completely eliminated.

Table 3. Lattice parameters of the Cr/$Fe_{65}Co_{35}$ bilayer samples determined from XRD data. The lattice parameters of bulk Cr and $Fe_{65}Co_{35}$ are also shown for comparison

Sample	***a*** (Å)
Cr (100 nm)/$Fe_{65}Co_{35}$ (10 nm)	2.92
Cr (100 nm)/$Fe_{65}Co_{35}$ (25 nm)	2.90
Cr (100 nm)/$Fe_{65}Co_{35}$ (50 nm)	2.89
Cr (100 nm)/$Fe_{65}Co_{35}$ (100 nm)	2.88
Bulk Cr [33]	2.88
Bulk $Fe_{65}Co_{35}$	2.85

3.3. Magnetic investigations

In order to investigate the magnetic properties of our films we recorded hysteresis loops between -1 and 1 T at temperatures between 4 and 300 K. Exchange bias can be induced either by applying a magnetic field during deposition or by cooling the sample in a constant field [15]. Our films were cooled from room temperature down to 4 K in an applied field of +0.3 T. The cooling field ensures that the $Fe_{65}Co_{35}$ layer magnetization is saturated during cooling, and the pinned Cr moments at the interface are aligned with the directions of the field and the magnetization of the $Fe_{65}Co_{35}$ layer [15]. Each hysteresis loop was recorded after field-cooling. The exchange bias field, H_E, and coercive field, H_C, were determined from the hysteresis loops and are defined as $H_E = (H_{RC} + H_{LC})/2$ and $H_C = (H_{RC} - H_{LC})/2$, respectively. H_{RC} and H_{LC} represent the right-hand and left-hand side coercive fields in the positive and negative field direction. A linear background was subtracted from the hysteresis loops due to the diamagnetic response of the Si(100)/SiO_2 substrate.

The hysteresis loops measured at 4 K with the field applied in-plane are shown in Figs. 6 (a) and (b).

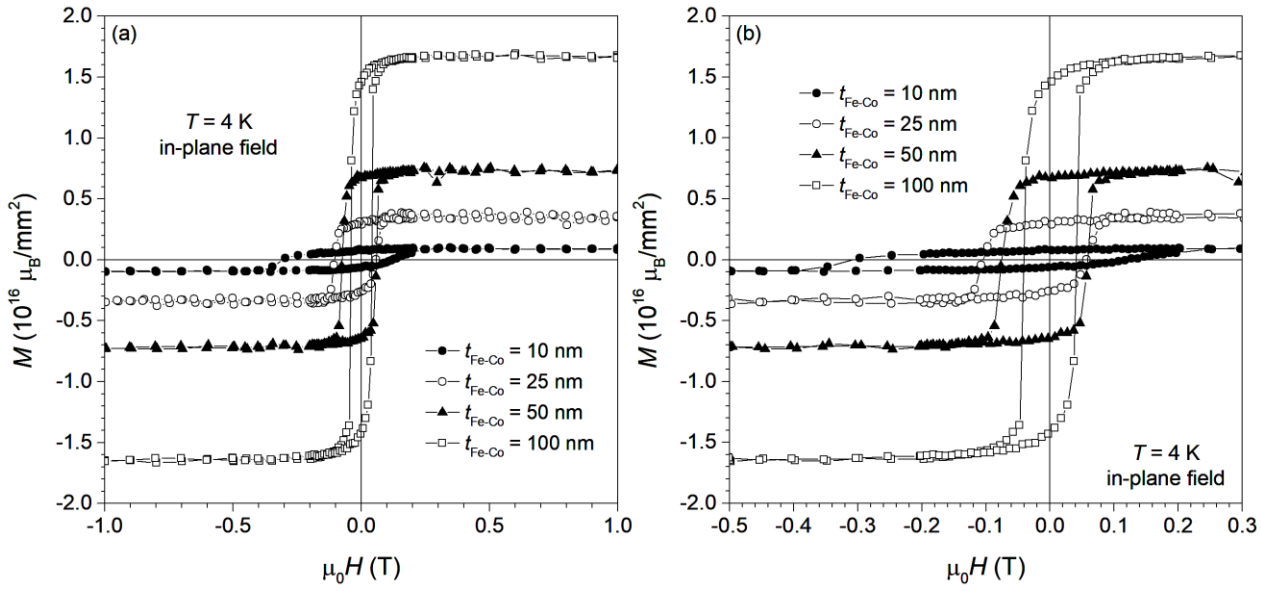

Fig. 6. (a) Hysteresis loops of the Cr/$Fe_{65}Co_{35}$ bilayer samples measured at 4 K between 1 and -1 T after field-cooling in +0.3 T from room temperature; (b) Zoom in on the same hysteresis loops between -0.5 and 0.3 T. The value $t_{Fe\text{-}Co}$ represents the $Fe_{65}Co_{35}$ layer thickness

By looking at the reversal curves we can see that switching occurs in a narrow field range, the easy magnetization axis lying in the plane of the films. With decreasing $Fe_{65}Co_{35}$ thickness the surface unit magnetization scales with the thickness. If the surface magnetization remained constant with decreasing thickness, then the magnetization would scale with the law $M(t_{Fe\text{-}Co}) = M(100)*0.01*t_{Fe\text{-}Co}$, where M is the magnetization of a sample with a given $Fe_{65}Co_{35}$ layer thickness, $t_{Fe\text{-}Co}$, and $M(100)$ corresponds to the surface

magnetization of the sample with a $Fe_{65}Co_{35}$ thickness of 100 nm. A linear fit of the saturation surface magnetization versus thickness yields a magnetization scaling law $M(t_{Fe\text{-}Co}) = M(100)*0.0097*t_{Fe\text{-}Co}$, therefore we can assume that the magnetization per unit volume of the films remains constant with decreasing thickness.

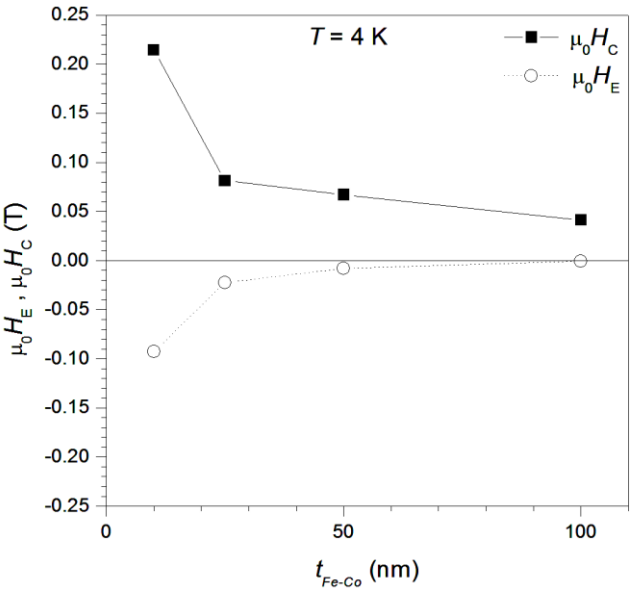

Fig. 7. Coercive field values, $\mu_0 H_C$, and exchange bias field values, $\mu_0 H_E$, measured at 4 K versus the $Fe_{65}Co_{35}$ layer thickness. The lines are guide for the eye

The coercive field values increase significantly with decreasing the $Fe_{65}Co_{35}$ thickness – Fig. 7. It is interesting to note that the hysteresis curves become increasingly asymmetric as the $Fe_{65}Co_{35}$ thickness drops below 50 nm. This indicates the presence of exchange bias in our samples, the exchange bias field increasing as the $Fe_{65}Co_{35}$ layer becomes thinner – Fig. 7. The loops are shifted along the field axis towards negative values, opposite to the direction of the setting field, i.e. we have negative bias. Therefore, we can deduce that the preferred magnetization direction of the bilayers is in the same direction as the setting field [15]. Exchange bias usually leads to an enhancement of the coercivity [15], which explains the increase of coercivity with decreasing $Fe_{65}Co_{35}$ thickness.

Exchange bias occurs due to the presence of uncompensated pinned AFM interfacial spins which, in the ground state, are aligned along the same direction as the FM spins. The pinned interfacial spins are anchored in the AFM layer through a Bloch domain wall [15]. The sign of the bias is given by the sign of the AFM/FM interfacial exchange coupling, while the size of the bias is dependent on several factors, such as the number of uncompensated pinned interfacial AFM spins, the exchange stiffness of the domain wall and the magnetocrystalline anisotropy of the AFM layer [15].

The exchange bias in Cr/$Fe_{65}Co_{35}$ films can be analyzed using a simple model given by Mauri et al. [15, 18, 37]. The model is illustrated in Fig. 8. We consider a bilayer sample consisting of a thick antiferromagnetic layer and a ferromagnetic layer of thickness t and magnetization M separated by an interface layer of thickness ξ (one to a few monolayers) [15, 18]. The AFM and FM layers are assumed to have a magnetocrystalline anisotropy along the x axis, with anisotropy constants K_{AFM} and K_{FM} respectively. The interface layer is comprised of uncompensated AFM spins, $\boldsymbol{S}_{\mathbf{AFM}}$, which are rigidly pinned to the AFM layer, and are aligned parallel to the ferromagnetic spins, $\boldsymbol{S}_{\mathbf{FM}}$ [15, 18].

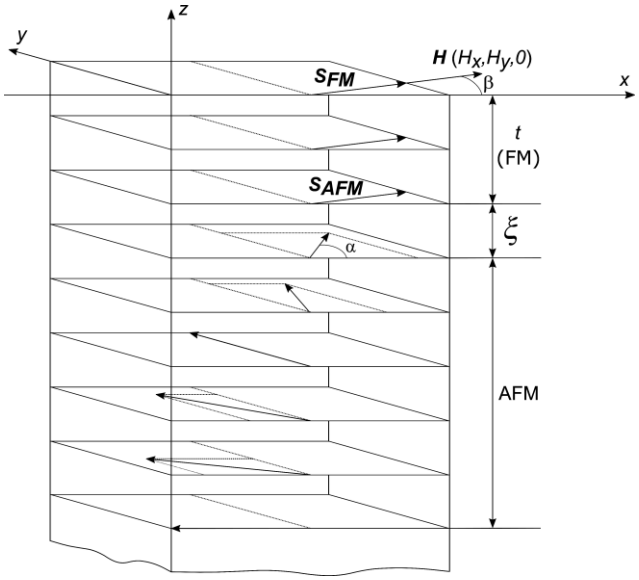

Fig. 8. Illustration of the model used for analyzing exchange bias in Cr/$Fe_{65}Co_{35}$ films [7, 19]. In the AFM only one spin sublattice is shown

The exchange coupling between FM and AFM interfacial spins is given by a Heisenberg-like coupling constant, J [15, 18]. If an external magnetic field $\boldsymbol{H}$ is applied at an angle β with respect to the x axis, the FM moments will align along the direction of the field. The uncompensated spins at the interface will be aligned at an angle α with respect to the x axis [15, 18]. If $\alpha \neq 0$, a Bloch wall tail will extend into the AFM [18]. The total magnetic energy per unit interface area, δ^*, is given by [15, 18]:

$$\delta^* = E_w(1-\cos\alpha) + \frac{JS_{AFM}S_{FM}}{a\xi}\left[1-\cos(\alpha-\beta)\right] + K_{FM}t\sin^2\beta + HMt(1-\sin\beta) \quad (1)$$

The first term in equation (1) is the energy of the domain wall tail extending into the AFM, E_w being the energy of a 90° domain wall. The second term in (1) represents the exchange coupling energy between $\boldsymbol{S}_{\mathbf{AFM}}$ and $\boldsymbol{S}_{\mathbf{FM}}$. This term can be positive or negative, depending on whether J is positive or negative. The third term represents the intrinsic FM magnetocrystalline anisotropy energy and the fourth term is the Zeeman energy.

The most common case is that of weak interfacial coupling, which is characterized by $\alpha \approx 0$ [15, 18]. In units of E_w, equation (1) becomes [15, 18]:

$$\delta = \mu_{\text{ani}} \sin^2 \beta + \kappa(1-\sin\beta) + \lambda_{\text{ex}}(1-\cos\beta) \qquad (2)$$

where $\lambda_{\text{ex}} = \frac{JS_{\text{AFM}}S_{\text{FM}}}{E_{\text{w}}a\xi}$ is the interface exchange, $\mu_{\text{ani}} = \frac{K_{\text{FM}}t}{E_{\text{w}}}$ is the anisotropy field, and $\kappa = \frac{HMt}{E_{\text{w}}}$ is the normalized field [18]. The last term in equation (2) introduces asymmetry in the hysteresis loops, due to the fact that we obtain different results for β = 0 and β = 180º [15]. The shift in the hysteresis loops is due to the transferred exchange bias field, H_{E} [15, 18]:

$$H_E = -\frac{JS_{\text{AFM}}S_{\text{FM}}}{a\xi tM} \qquad (3)$$

Usually, the bias field values are overestimated [15] because in the model an entire interface layer of uncompensated AFM spins is assumed. It was previously shown that in reality only a fraction of interfacial spins is pinned [15, 38-40]. Therefore, the exchange bias in equation (3) must be multiplied with a scaling factor, as the pinned interfacial spin density, $S_{\text{AFM}}/a\xi$, is reduced.

The measured and calculated exchange bias field values versus $Fe_{65}Co_{35}$ thickness are shown in Fig. 9 (a). Indeed, the exchange bias field is inversely proportional to the thickness, decreasing as 1/*t*. For the calculation of the bias field using Mauri's model we used *J* value of 10 meV, corresponding to a pair of atoms [15], which was assumed to remain unchanged with $Fe_{65}Co_{35}$ thickness. For the interface layer thickness, we used $\xi = a$ = 0.249 nm, i.e. the nearest-neighbour distance in Cr, or one atomic layer.

From the magnetization curves, a magnetization value of M = 166 μ_B/nm^3 was obtained for a $Fe_{65}Co_{35}$ thickness of 100 nm corresponding to a magnetic moment of 1.98 μ_B/atom.

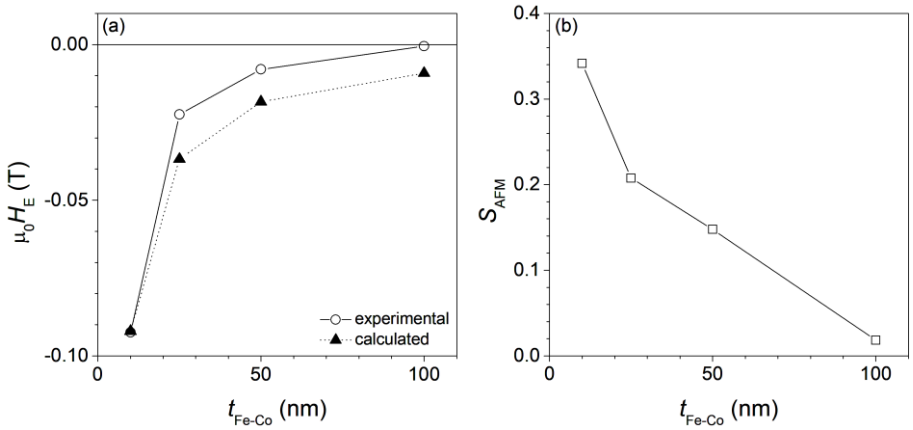

Figure 9. (a) Measured (T = 4 K) and calculated exchange bias field values versus $Fe_{65}Co_{35}$ thickness; (b) calculated interface antiferromagnetic spin value, S_{AFM} versus $Fe_{65}Co_{35}$ thickness. The lines are guide for the eye

As we stated before, we assume a constant magnetization with varying thickness. This leads us to a ferromagnetic spin value of S_{FM} of 0.99. Band structure calculations showed a Cr spin value between 0.10 and 0.34. At the Cr/$Fe_{65}Co_{35}$ interface we have reduced coordination, which could lead to an enhanced magnetic moment of the interface Cr layer as observed elsewhere [41]. Therefore, for the antiferromagnetic spin value we can assume the maximum value determined from band structure calculations, S_{AFM} = 0.34. For the sample with a $Fe_{65}Co_{35}$ thickness of 10 nm, the model yields an overestimated bias field value of 0.57 T, while the experimental value is around 0.09 T. However, if we consider a reduced interfacial spin density, by using a scaling factor of 0.16, the model yields an exchange bias field value close to the experiment. It was previously reported that usually only around 4-7% of the interfacial spins are pinned, so the scaling factor has values around 0.04-0.07 [15, 38-40]. The scaling factor in our case is of the same magnitude but slightly higher than previously reported values, possibly due to strain and the rough Cr/$Fe_{65}co_{35}$ interface, which could create an increased surface density of pinning centers. With increasing thickness, we can see that for the samples with 25, 50 and 100 nm of $Fe_{65}Co_{35}$ the calculated bias fields are still overestimated. Interestingly, the difference between the calculated and experimental bias field values decreases with increasing $Fe_{65}Co_{35}$ thickness. As we assumed the parameters *J*, *M*, *a*, ξ, and S_{FM} to be constant, the possible causes for this behavior are either a decrease in the fraction of pinned interfacial AFM spins with the thickness, or a decrease of the interface AFM spin value S_{AFM}. On one hand, as the films were deposited in the same conditions (technique, substrate, temperature, sputtering power, Ar pressure), the interfacial defect density on which the AFM spins are pinned could be assumed the same for all four samples. In other words, the scaling factor should have the same value for all of the samples. On the other hand, band structure calculations showed that the interface Cr magnetic moment decreases as more $Fe_{65}Co_{35}$ layers are added to the system. Therefore, we can infer that the difference between the calculated and experimental bias field values is determined by decreasing S_{AFM} values with $Fe_{65}Co_{35}$ thickness. By

using the experimental H_E values in equation (3) multiplied with a scaling factor of 0.16, we calculated the interface AFM spin values, S_{AFM}. The results show that S_{AFM} decreases with $Fe_{65}Co_{35}$ thickness – Fig. 9 (b) – in agreement with the theoretical results.

The magnetic behavior of the samples at different temperatures was also investigated by means of hysteresis curves recorded after field-cooling the samples in +0.3 T from room temperature to the respective temperature value. Hysteresis loops recorded at different temperatures for the investigated samples are shown in Fig. 10. For the sample with a $Fe_{65}Co_{35}$ thickness of 100 nm – Figure 10a – the hysteresis curves are symmetric, and the coercive field decreases upon increasing temperature. With decreasing thickness, at low temperatures, the curves become more asymmetric, due to the increase of the bias field with $Fe_{65}Co_{35}$ thickness – Figs. 10 (b), (c), and (d). With increasing temperature, the right and left-hand side coercive fields decrease. For the sample with 100 nm of $Fe_{65}Co_{35}$, the right-hand side and left-hand side coercive field values decrease at the same rate with temperature, the hysteresis curves remaining symmetric. For the samples with 50, 20 and 10 nm of $Fe_{65}Co_{35}$ respectively, the left-hand side coercive fields decrease at a faster rate than the right-hand side ones. This can be attributed to a decrease of both the exchange bias and coercive fields upon increasing temperature.

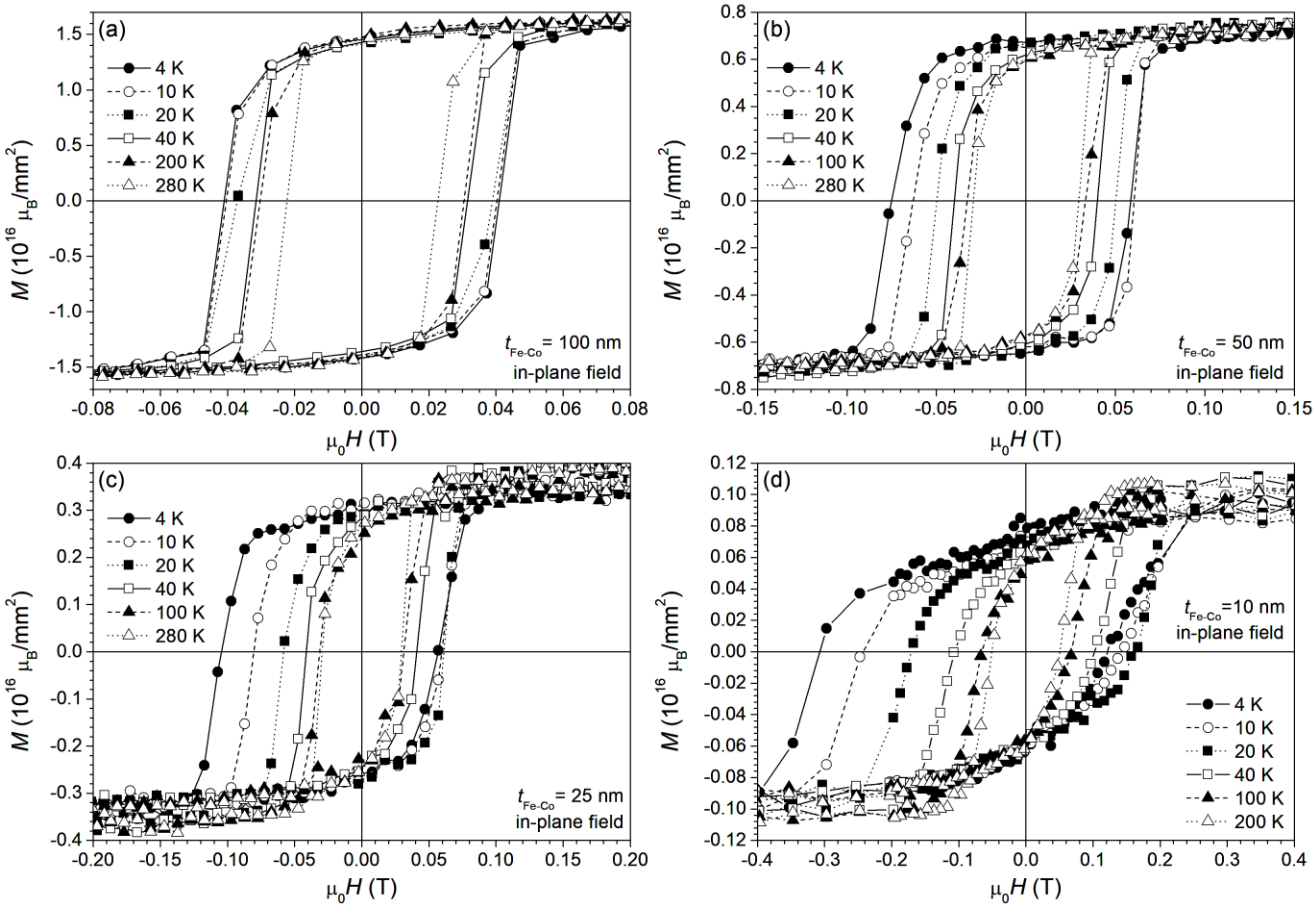

Fig. 10. Hysteresis loops measured between 1 and -1 T at different temperatures after field-cooling in 0.3 T from room temperature for the samples having a $Fe_{65}Co_{35}$ thickness of: (a) 100 nm, (b) 50 nm, (c) 25 nm and (d) 10 nm

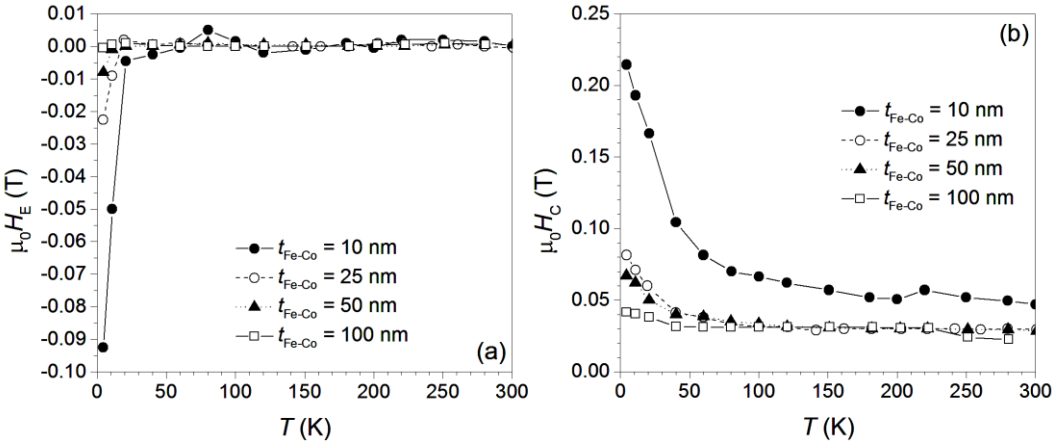

Fig. 11. Exchange bias field (a) and coercivity (b) values for all of the Cr/ $Fe_{65}Co_{35}$ bilayer samples. The lines are guide for the eye

The temperature dependence of the exchange bias field for different $Fe_{65}Co_{35}$ thicknesses is shown in Fig. 11 (a). The bias field decreases rapidly with temperature and becomes 0 around the blocking temperature, T_B = 20 K. The fact that T_B is smaller than the Neel temperature, T_N, would suggest that the ISDW phase is present in the Cr layer [8]. Also, in epitaxial Cr/Fe films, a spin-flip transition, from $\mathbf{S}_{AFM} \| \mathbf{Q}$ to $\mathbf{S}_{AFM} \perp \mathbf{Q}$, was reported similar to bulk Cr, which is identified as a peak in the coercivity versus temperature [8]. Also, an oscillation of the bias field with temperature was reported for epitaxial Cr/Fe films, which was attributed to the modulation of the ISDW wavelength with temperature [8]. Our samples do not display an oscillating bias field with temperature nor do they show a spin-flip transition in the coercivity – Fig. 11 (b). It was suggested that interface disorder, such as strain and interface roughness could cause a commensurate SDW at the interface, which can lead to unusually large bias field values and an absence of both the $\mu_0 H_E$ oscillation and the spin-flip transition [31]. The large bias field values and the presence of strain in our samples could indicate that the commensurate SDW phase is present in the Cr layer. In Cr/Fe systems, the reported bias field values range from 0.001 to 0.01 T, or 10 Oe to 100 Oe [8, 31]. The bias field value of 0.09 T obtained in the sample with 10 nm is around one to two orders of magnitude larger than the previously reported values. The large bias field value could be attributed to two factors. First, the higher magnetization of $Fe_{65}Co_{35}$ could lead to an enhanced bias field value. Second, the rough surface and the presence of strain could generate a high pinning center density, which could also enhance the bias field by increasing the antiferromagnetic spin density at the interface. The decrease of the bias field with temperature and its vanishing at T_B could be explained by the fact that although Cr is antiferromagnetic up to the Neel temperature, thermal fluctuations can cause the interface exchange coupling between interfacial FM and AFM spins to become random, decreasing the bias field [31].

The coercivity values decrease with temperature and increase as the films get thinner. For the samples with a $Fe_{65}Co_{35}$ thickness of 25, 50 and 100 nm, the coercive field decreases and remains constant after 60 K at a value around 0.03 T. By contrast, for the sample with 10 nm of $Fe_{65}Co_{35}$ the coercive field also decreases with temperature, however, it decreases slowly after 60 K and is almost double the value obtained for the other three samples. This could be explained by the fact that as the $Fe_{65}Co_{35}$ thickness is very low, it could lead to an enhanced anisotropy, which in turn leads to higher coercivity values.

4. Conclusions

In summary, the effect of the $Fe_{65}Co_{35}$ thickness on the magnetic properties of Cr/$Fe_{65}Co_{35}$ thin films was investigated both theoretically and experimentally. Electronic structure calculations showed that Co addition and the deposition of multiple layers dampens the Cr moments in the underlayer, leading to a decrease of the spin moment at the interface. Experimentally, the magnetic properties were investigated from hysteresis curves performed on thin film samples, which were field cooled in an applied field of +0.3 T. Negative exchange bias was found in all of the samples, and the magnitude of the exchange bias field at 4 K was found to be inversely proportional to the $Fe_{65}Co_{35}$ thickness. The largest exchange bias field of 0.09 T was found at 4 K for the sample with a $Fe_{65}Co_{35}$ thickness of 10 nm. A simple model was used to analyze the exchange bias in Cr/$Fe_{65}Co_{35}$ bilayers, which pointed out the fact that as the $Fe_{65}Co_{35}$ thickness increased, the interface antiferromagnetic spin moment decreased, in agreement with theoretical results. The high bias field values and the presence of strain and interface roughness in our samples pointed to the possibility of a commensurate SDW phase at the Cr/$Fe_{65}Co_{35}$ interface.

Acknowledgements

This work was supported by the Romanian Ministry of Education and Research, Grant PN-II-RU-TE-2014-4-2360. The authors acknowledge the Romanian-French

cooperation program Brancusi, Grant PN-III-P3-3.1-PM-RO-FR-2016-0057.

References

[1] J. Nogués, I. K. Schuller, J. Magn. Magn. Mater. **192**, 203 (1999).
[2] V. Skumryev, S. Stoyanov, Y. Zhang, G. Hadjipanayis, D. Givord, J. Nogués, Nature **423**, 850 (2003).
[3] C. Chappert, A. Fert, F. N. van Dau, Nature Mater. **6**, 813 (2007).
[4] L. Anghinolfi, F. Bisio, M. Canepa, L. Mattera, Phys. Rev. B **81**, 224427 (2010).
[5] W. Zhang, K. M. Krishnan, Mat. Sci. Eng. R **105**, 1 (2016).
[6] M.-H. Phan, J. Alonso, H. Khurshid, P. Lampen-Kelley, S. Chandra, K. S. Repa, Z. Nemati, R. Das, Ó. Iglesias, H. Srikanth, Nanomater. **6**, 221 (2016).
[7] F. Y. Yang, C. L. Chien, J. Appl. Phys. **93**, 6829 (2003).
[8] J. S. Parker, L. Wang, K. A. Steiner, P. A. Crowell, C. Leighton, Phys. Rev. Lett. **97**, 227206 (2006).
[9] E. Fawcett, Rev. Mod. Phys. **60**, 209 (1988).
[10] S. S. P. Parkin, N. More, K. P. Roche, Phys. Rev. Lett. **64**, 2304 (1990).
[11] E. E. Fullerton, D. M. Kelly, J. Guimpel, I. K. Schuller, Y. Bruynseraede, Phys. Rev. Lett. **68**, 859 (1992).
[12] R. W. Wang, D. L. Mills, E. E. Fullerton, J. E. Mattson, S. D. Bader, Phys. Rev. Lett. **72**, 920 (1994).
[13] M. Rührig, R. Schäfer, A. Hubert, R. Mosler, J. A. Wolf, S. Demokritov, P. Grünberg, Phys. Status Solidi A **125**, 635 (1991).
[14] W. H. Meiklejohn, C. P. Bean, Phys. Rev. **102**, 1413 (1956).
[15] J. Stöhr, H. C. Siegmann, Magnetism from Fundamentals to Nanoscale Dynamics, Springer-Verlag Berlin Heidelberg, 617, 2006.
[16] K. Gandha, R. P. Chaudhary, J. Mohapatra, A. R. Koymen, J. Ping Liu, Phys. Lett. A **381**, 2092 (2017).
[17] Y. X. Gao, C. M. Zhu, S. Huang, Z. M. Tian, S. L. Yuan, J. Magn. Magn. Mater. **439**, 348 (2017).
[18] D. Mauri, H. C. Siegmann, P. S. Bagus, E. Kay, J. Appl. Phys. **62**, 3047 (1987).
[19] P. Grünberg, R. Schreiber, Y. Pang, M. B. Brodsky, H. Sowers, Phys. Rev. Lett. **57**, 2442 (1986).
[20] D. Aernout, C. L'abbé, M. Rots, H. Fritzsche, J. Meersschaut, Phys. Rev. B **73**, 134419 (2006).
[21] K. Schwarz, P. Mohn, P. Blaha, J. Kübler, J. Phys. F: Met. Phys. **14**, 2659 (1984).
[22] A. V. Trifu, E. Dorolti, A. F. Takacs, I. Chicinaş, O. Isnard, V. Pop, Mat. Sci. Eng. B **178**, 1352 (2013).
[23] T. Sourmail, Prog. Mater. Sci. **50**, 816 (2005) 816.
[24] M. Delshad Chermahini, M. Zandrahimi, H. Shokrollahi, S. Sharafi, J. Alloys. Compd. **477**, 45 (2009).
[25] H. Ebert, D. Ködderitzsch, J. Minár, Rep. Prog. Phys. **74**, 096501 (2011).
[26] R. Zeller, P. H. Dederichs, B. Újfalussy, L. Szunyogh, P. Weinberger, Phys. Rev. B **52**, 8807 (1995).
[27] S. H. Vosko, L. Wilk, M. Nusair, Can. J. Phys. **58**, 1200 (1980).
[28] M. Björck and G. Andersson, J. Appl. Cryst. **40**, 1174 (2007).
[29] T. Furubayashi, I. Nakatani, N. Saegusa, J. Phys. Soc. Jpn. **56**, 1855 (1987).
[30] O. Isnard, D. Fruchart, J. Alloys Compd. **205**, 1 (1994).
[31] K.-Y. Kim, S.-C. Shin, Y.-S. Hwang, Y. Jo, S. Angappane, J.-G. Park, J. Kor. Phys. Soc. **54**, 175 (2009).
[32] R. T. Downs, D. C. Palmer, Am. Mineral. **79**, 9 (1994).
[33] Y. C. Feng, D. E. Laughlin, D. N. Lambeth, J. Appl. Phys. **76**, 7311 (1994).
[34] M. T. Hosseinnejad, M. Ettehadi-Abari, N. Panahi, M. A. Ferdosi Zadeh, S. W. Case, J. Optoelectron. Adv. M., **19**, 434 (2017).
[35] T.-T. Liang, A.-Q. Wang, H.-L. Zhao, J.-P. Xie, Optoelectron. Adv. Mat., **11**, 574 (2017).
[36] H. E. Swanson, N. T. Gilfrich, G. M. Ugrinic, National Bureau of Standards Circular **539**, V, 20 (1955).
[37] R. Skomski, Simple Models of Magnetism, Oxford University Press, New York, 268, 2008.
[38] H. Ohldag, A. Scholl, F. Nolting, E. Arenholz, S. Maat, A. T. Young, M. Carey, J. Stöhr, Phys. Rev. Lett. **91**, 017203 (2003).
[39] P. Kappenberger, S. Martin, Y. Pellmont, H. J. Hug, J. B. Kortright, O. Hellwig, E. E. Fullerton, Phys. Rev. Lett. **91**, 267202 (2003).
[40] L. C. Sampaio, A. Mougin, J. Ferré, P. Georges, A. Brun, H. Bernas, S. Poppe, T. Mewes, J. Fassbender, B. Hillebrands, Europhys. Lett. **63**, 819 (2003).
[41] P. J. Jensen, K. H. Bennemann, Langmuir **12**, 45 (1996).

*Corresponding author: sever.mican@phys.ubbcluj.ro